

Anodic processes in plasma electrolytic oxidation of aluminium in alkaline solutions

L.O. Snizhko^a, A.L. Yerokhin^{b,*}, A. Pilkington^b, N.L. Gurevina^a,
D.O. Misnyankin^a, A. Leyland^b, A. Matthews^b

^a Ukrainian State University for Chemical Engineering, 8 Gagarin Avenue, Dnepropetrovsk 49027, Ukraine

^b Department of Engineering Materials, University of Sheffield, Mappin Street, Sheffield S1 3JD, UK

Received 17 July 2003; received in revised form 29 October 2003; accepted 28 November 2003

Abstract

In this paper, basic electrochemical processes (such as oxide film growth, anodic dissolution and oxygen liberation) on an aluminium anode in a model alkaline solution are considered under conditions of galvanostatic DC plasma electrolytic oxidation (PEO). The experiments performed include: (i) recording and analysis of the main electrical characteristics of the process; (ii) determination of the oxide layer thickness; (iii) anodic gas collection and composition analysis and (iv) electrolyte analysis to determine dissolved aluminium. Four different stages of the PEO process have been identified, characterised by various rate proportions of the partial anodic processes. Overall current efficiency of the oxide film formation has been estimated to be in the 10–30% range. The film growth rate decreases significantly with increasing electrolyte concentration from 0.5 to 2 g l⁻¹ KOH, since the rate of anodic dissolution increases. Oxygen evolution is shown to be the main electrochemical process at the potentials corresponding to the plasma stages of the electrolysis. The overall rate of oxygen liberation at the anode exceeds the Faraday yield, which is probably due to the radiolytic effect of the plasma discharge on the adjacent electrolyte volume. © 2003 Published by Elsevier Ltd.

Keywords: Plasma electrolytic oxidation; Oxide film; Anodic dissolution; Oxygen liberation; Plasma discharge

1. Introduction

Plasma electrolytic oxidation (PEO) of metals is a complex process combining concurrent partial processes of oxide film formation, dissolution and dielectric breakdown. The probability of dominance for any of these partial processes in the overall process depends on the nature of both the metal and the electrolyte, as well as on the current regime employed. The ultimate stage of the PEO treatment is a quasi-stationary state of persistent anodic microdischarges, which exhibit a progressive change in characteristics during the electrolysis. At high discharge temperatures and pressures (reaching about 2×10^3 to 3×10^3 °C and $\sim 10^2$ MPa, respectively), solid products of electrolysis and adsorbed gel layers are deposited on the metal surface in the form of high-temperature oxide phases or glassy ceramic

coatings [1]. Depending on the purpose, the PEO treatment is typically carried out for between 5 and 180 min at current densities of 500–2000 A m⁻² and voltages of up to 1000 V. The electrolysis is always accompanied by intensive gas evolution and localised metal evaporation due to the plasma thermochemical reactions in the microdischarges [2–11]. PEO is thus an energy-intensive process, and under these circumstances the issue of process efficiency becomes very important. Existing data in the literature on the energy efficiency of PEO are quite controversial (Table 1). Such a wide scatter in the data suggests that certain side processes take place on the oxidising surface, the role of which in plasma electrolysis is yet to be understood. Careful determination of the material balance at the metal electrode, is therefore, required to evaluate the efficiency of the PEO process.

To produce PEO coatings on aluminium, alkaline electrolytes are widely used, containing silicates, aluminates, polyphosphates, etc. [2–5,10,11], which can passivate the metal surface due to the formation of near-surface gels [12] or insoluble compounds [13]. However, such electrolytes are

* Corresponding author. Tel.: +44-1142225466; fax: +44-1142225943.
E-mail address: A.Yerokhin@sheffield.ac.uk (A.L. Yerokhin).

Table 1
Comparative data of current efficiency in plasma electrolytic oxidation

Anode material	Electrolyte	Electrolysis parameters			Oxide yield $\eta_{\text{Me}_x\text{O}_y}$ (%)	Reference
		t (°C)	i (A m^{-2})	τ (s)		
Al	H_2SO_4 (concentrated)	10–24	1350	1400	57	[9]
	$\text{Na}_2\text{O}\cdot 3\text{SiO}_3$ (40 g l^{-1})	25	250	360	9.1	[2]
Ti	H_2SO_4 (1 mol l^{-1})	25	100	1000–5000	11–21	[8]
	$\text{Na}_3\text{PO}_4\cdot 12\text{H}_2\text{O}$	20	536	180	74	[4]

not ideally suited to material balance evaluations for the following reasons:

- passivating anions inhibit the process of aluminium dissolution, masking mechanism changes in anodic reactions during plasma electrolysis;
- chemical analysis of such complex electrolytes and coatings produced is quite difficult;
- the oxidation kinetics are affected by the electrolyte components incorporated into the oxide film [13,16–18].

It is reasonable, therefore, to reduce the electrochemical system under consideration to a simple model situation, in which aluminium is oxidised in a dilute alkaline electrolyte without any passivating anions. The primary objective of this study was to evaluate the oxide film growth efficiency during different stages of PEO treatment of aluminium in $0.5\text{--}2.0 \text{ g l}^{-1}$ solutions of KOH. For this purpose, a series of experiments on plasma electrolytic oxidation has been performed, which included time-resolved determination of the following characteristics: (i) evolution rate and composition of anodic gaseous products; (ii) rates of aluminium chemi-

cal and anodic dissolution in the electrolyte and (iii) oxide coating growth rate, structure and phase composition.

2. Experimental

2.1. Electrolysis

A schematic of the experimental set-up used in this work is shown in Fig. 1. Samples made from a 6082 aluminium alloy (contained 0.6% Mg; 1% Si; 0.7% Mn, as basic alloying elements) were used having a total surface area of $1.23 \times 10^{-3} \text{ m}^2$. A preliminary mechanical polishing was given to the sample surfaces to achieve a R_a of $\sim 0.1 \mu\text{m}$, followed by a degreasing in methyl alcohol. The oxidation process was carried out in a 2-l glass vessel equipped with a coil heat exchanger and a magnetic stirrer. The samples were suspended in the electrolyte using a rigid threaded contact insulated from the electrolyte by a plastic jacket and covered with an inverted glass funnel which served to collect anodic gases during the plasma electrolysis. A stainless steel ring

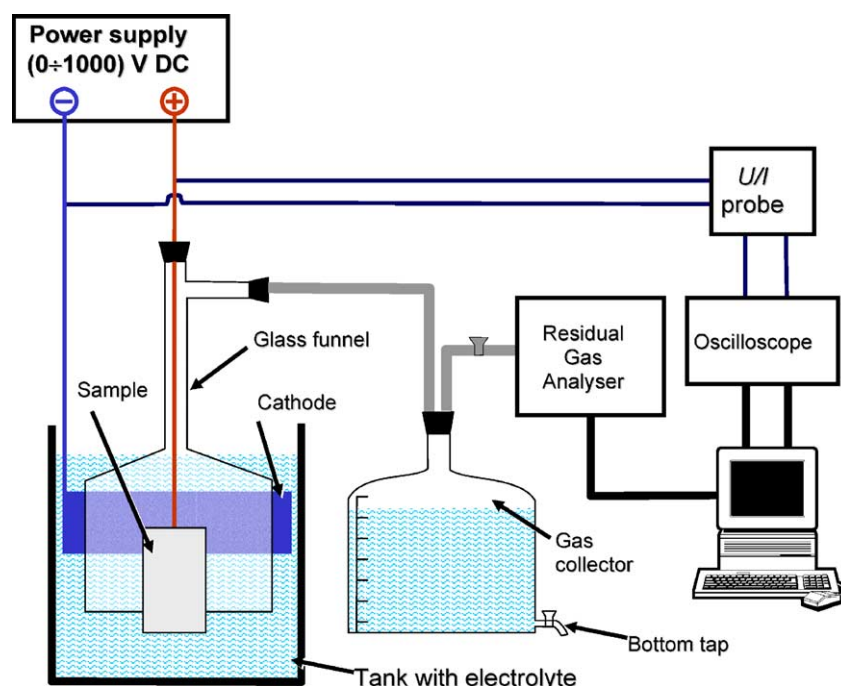


Fig. 1. Layout of the experimental set-up.

cathode with surface area of $5.75 \times 10^{-2} \text{ m}^2$ was positioned above the funnel to prevent cathodic gases from entering the anolyte area. The galvanostatic regime of DC PEO was employed with current density i set in the 467 to 1407 A m^{-2} range.

Aqueous solutions of KOH with $0.5\text{--}2.0 \text{ g l}^{-1}$ concentration were chosen as electrolytes. The concentrations employed in this work were verified during pre-experimentation, which showed that beyond them, the breakdown voltage either exceeds 1000 V due to reduced conductivity of more diluted solutions, or cannot be achieved at all due to intensive dissolution of the anode in more concentrated electrolytes. Electrolyte temperature, as monitored prior to and after the electrolysis, was always kept within the range $15\text{--}45^\circ\text{C}$.

2.2. Anodic gas analysis

During the electrolysis, anodic gas was collected into the glass vessel filled with water (Fig. 1). The vessel was initially sealed, i.e. air pressure in the neck pipe was equalised by atmospheric pressure from the open bottom tap side, preventing water from leaking out of the vessel. Anodic gas evolved during the electrolysis was accumulated in the top section of the vessel, displacing a correspondent volume of water via the bottom tap; this volume was measured to evaluate the gas evolution rate. To minimise the possibility of gas dissolution in both the electrolyte and the water, the entire system was purged with oxygen for about 30 min prior to each experiment. The volume V_t of the collected humid gas was reduced to the normal (STP) conditions according to the following formula [8]:

$$V = \frac{(P - p_t)V_t \times 273}{1.01325 \times 10^5(273 + t)} \quad (1)$$

Here P and t are laboratory pressure and temperature, respectively; p_t is saturated vapour pressure at the given temperature [19].

The composition of the collected gas was studied using a Spectramass Data Quad Type DAQ 3.2 quadrupole residual gas analyser operated at 0.4 Pa. The mass channels corresponding to H_2 , N, O, H_2O , N_2 , O_2 , Ar and O_3 were monitored and the data from five parallel measurements for each channel were averaged to obtain the percentage of the corresponding substance in the gas mixture.

2.3. Electrolyte analysis

After the oxidation, electrolyte solutions were analysed for the presence of dissolved aluminium using a Perkin Elmer Plasma 40 emission ICP OES instrument. Three replicate measurements from each solution were taken at the emission wavelength of 396.152 nm, with uptake and washout times being 60 s each. The results were quantified with respect to a calibration line, which has been obtained using 0, 1, 5 and 10 ppm standard solutions prepared from

a certified 1000 ppm solution. Some samples containing more than 20 ppm of dissolved Al were diluted as appropriate, then the results were corrected for the dilution. Another correction was performed for the blank sample value (0.076 ppm), which was subtracted from the initial results.

2.4. Chemical dissolution of aluminium

The chemical dissolution rate of the substrates immersed in the electrolyte solutions was evaluated by the sample weight loss, with time and temperature conditions kept similar to those used for the plasma electrolysis experiments. The weight loss was measured with $\pm 0.1 \text{ mg}$ accuracy using a Mettler H31AR analytical balance. These data were taken into account prior to calculation of the rate of Al anodic dissolution due to electrochemical processes during PEO.

2.5. Oxide film growth rate

The oxide layer growth rate was determined from the layer thickness measurements performed on polished cross-sections using conventional optical microscopy techniques. Several parallel measurements (typically 15–20) were taken across the sample cross-section perimeter in order to provide statistically significant data of the film thickness. Based on these data, mass yield of aluminium oxide formed during plasma electrolysis was calculated, assuming that oxide density $\rho = 3100 \text{ kg m}^{-3}$ [1].

3. Results

3.1. (U ; τ) dependencies

The galvanostatic dependencies of anode voltage (U) on PEO treatment time (τ) obtained at different chosen current densities and electrolyte concentrations are shown in Fig. 2a and b. In the general case, four characteristic areas can be resolved in the dependencies, evidencing changes in the mechanisms of the anodic process. Inset in Fig. 2a shows a typical example of linear approximations of the (U ; τ) curves in the above regions, which can be characterised as follows. Region (I) exhibits maximum gradient on the voltage curve, corresponding to a conventional aluminium anodising process. In region (II), the rate of voltage increase slackens, indicating a decrease in the oxide film growth rate; oxygen bubbles first appear on the sample surface in this region. With increasing current density, the temporal duration of region (II) diminishes and becomes practically indistinguishable at $i = 1407 \text{ A m}^{-2}$ (Fig. 2a). In region (III), the rate of voltage increase rises again; this usually corresponds to oxide recrystallisation and defect appearance in the film structure [14].

Region (IV) begins with intensive oxygen evolution, which creates a background for the onset of plasma microdischarge phenomena at the sample surface. The process

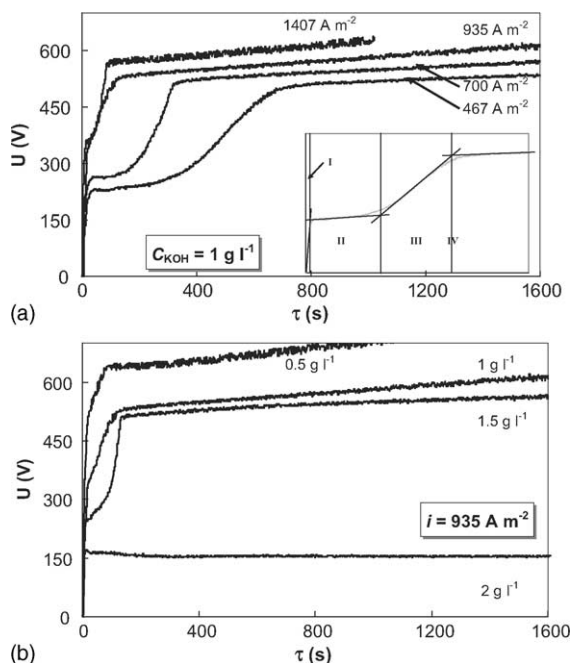


Fig. 2. Voltage vs. time plots under different conditions of PEO, illustrating (a) effect of current density. The inset shows a typical pattern of linear approximation for (U ; τ) dependencies with four stages of the process resolved; (b) effect of electrolyte concentration.

becomes more steady-state, with only changes in the discharge appearance observed, which progresses gradually from a dense population of small and frequent microdischarges towards smaller populations of larger and longer-lived discharge events. The threshold voltage at which the plateau in region (IV) is entered decreases with increasing electrolyte concentration (Fig. 2b) and ultimately cannot be achieved at 2 g l^{-1} KOH, due (probably) to the prevailing rapid dissolution of the oxide film.

3.2. Anodic gas evolution

The anodic gas composition was found to consist predominantly of oxygen (>93%) with minor amounts of hydrogen (about 2%) and some residual nitrogen (<4%), which probably remained in pipelines of the experimental rig (particularly in the part shown in grey in Fig. 1). Nevertheless, nitrogen content reduced substantially with increase in total volume of the anodic gas and was not affected by the process parameters, i.e. current density or electrolyte concentration. The effect of these parameters on the kinetics of gas evolution is shown in Fig. 3a and b. Commencement of intensive gas evolution always coincides with the onset of a plasma discharge on the electrode surface. It can be seen that all the dependencies are linear, with gradients defined by the electrolysis parameters. The gas evolution rate increases substantially with increasing current density, whereas it is almost independent of electrolyte concentration in the range of $0.5\text{--}1.5 \text{ g l}^{-1}$ but decreases sharply in 2 g l^{-1} KOH solution.

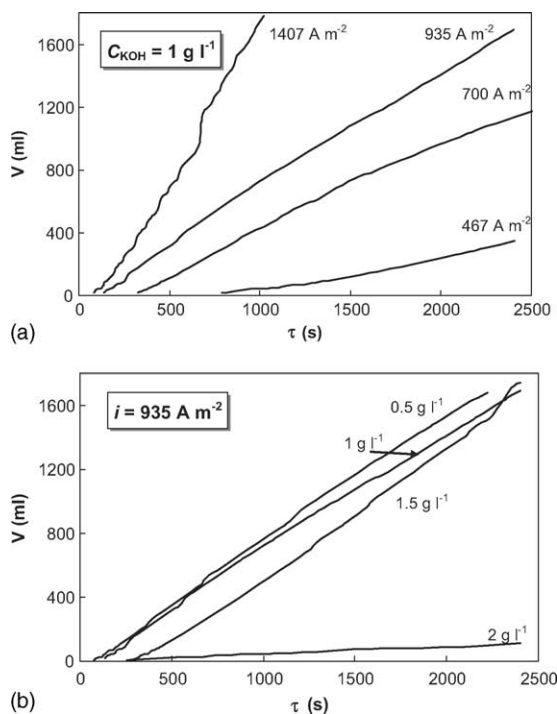


Fig. 3. Kinetics of gas evolution during PEO. (a) Effect of current density; (b) effect of electrolyte concentration.

The charge density passed through the electrolyser before the onset of discharge activity at the oxide surface is shown in Fig. 4a and b, illustrating effects of current density and electrolyte concentration, respectively. The charge consumed in the pre-discharge stages increases with higher electrolyte concentration and decreases with increased current density. Indeed, the more extended are regions (II)

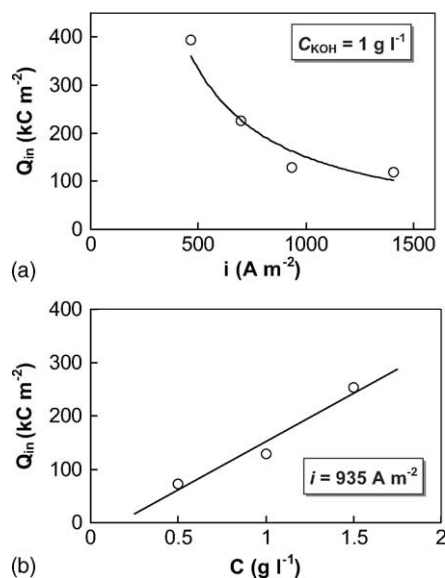


Fig. 4. Effect of process parameters, e.g. (a) current density and (b) electrolyte concentration on the value of charge density Q_{in} required to onset the conditions of plasma discharge at the anode surface.

and (III), the more difficult the breakdown voltage is to achieve and the more significant is the contribution of the aluminium dissolution partial process to the net oxidation kinetics.

3.3. Aluminium dissolution

In Fig. 5, typical dependencies for the rate of anodic dissolution of aluminium $(dm_{Al}/d\tau)^{an}$ on the PEO process parameters, such as charge passed through the electrolyser (Fig. 5a) and electrolyte concentration (Fig. 5b) are shown, along with data for Al chemical dissolution in KOH solution (Fig. 5c). It should be pointed out that although metal dissolution occurs in all studied cases, the effect of current

density is more pronounced in the earlier stages of the process. Additionally, the rates of both chemical and electrochemical dissolution reactions are affected by the alkaline electrolyte concentration.

Changes in the electrolyte pH observed during the PEO experiments indicate electrolyte acidification proportional to the charge passed through the system, which is more noticeable at higher current densities (Fig. 6a). Surprisingly, it appears that the electrolyte acidification develops only at the plasma electrolytic stage, since in 2 g l^{-1} KOH solution, where discharge conditions could not be achieved, the electrolyte pH remains unchanged—despite the substantial duration of the oxidation process, i.e. 40 min (Fig. 6b).

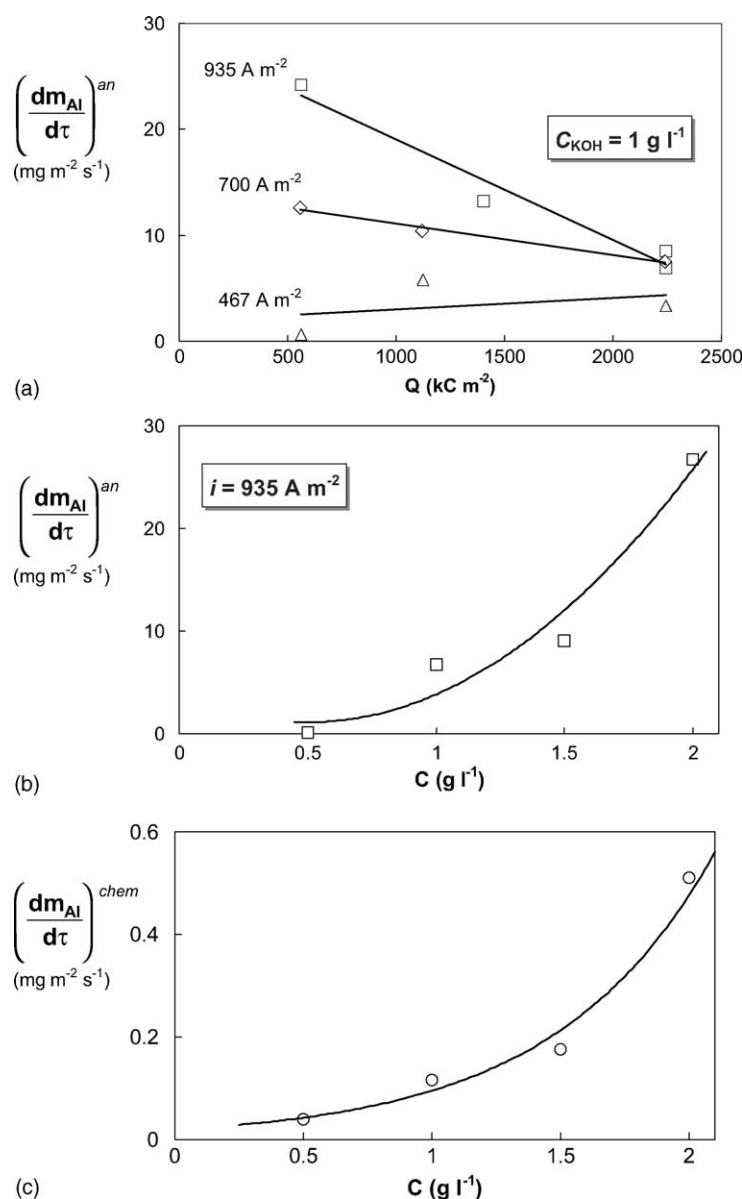


Fig. 5. Effect of PEO parameters on aluminium content in KOH solutions: (a) effect of current density; (b) and (c) effects of electrolyte concentration on anodic and chemical dissolution of Al, respectively (time of electrolysis is 40 min).

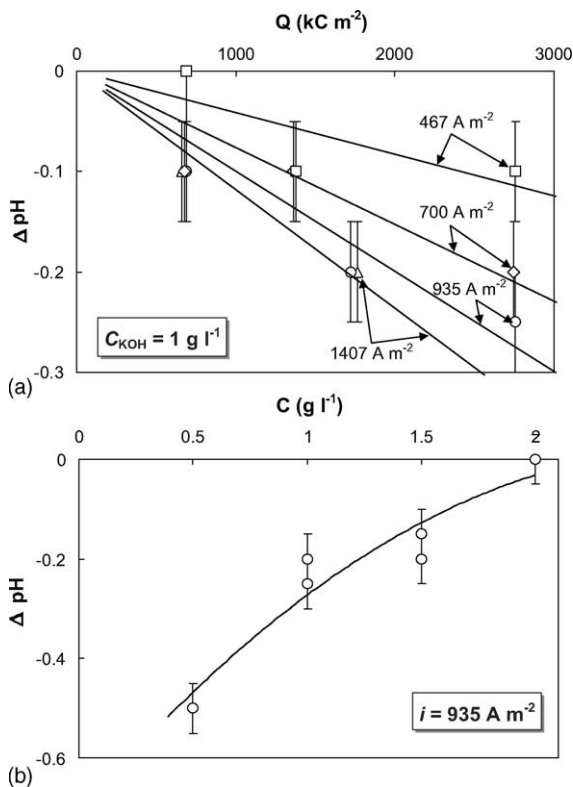


Fig. 6. Effect of PEO parameters on the electrolyte pH: (a) effect of charge density; (b) effect of electrolyte concentration (time of electrolysis is 40 min).

3.4. Oxide layer thickness

Typical relationships between oxide layer thickness and PEO process parameters are shown in Fig. 7a and b. Generally, the layer thickness increases with charge passed through the sample surface, although the character of this trend is different for lower ($\leq 699 \text{ A m}^{-2}$) and higher ($\geq 935 \text{ A m}^{-2}$) current densities (Fig. 7a). In the case of the former, the layer grows almost linearly throughout the process whereas in the latter, almost no thickness increase is observed in the 700–1800 kC m^{-2} charge density range but in the final stages the increase is substantial. Dependence of thickness on the electrolyte concentration displays a maximum growth rate at 1 g l^{-1} KOH (Fig. 7b). At lower concentrations, the electrolytic oxidation process is probably less efficient and at higher ones the effect of the partial process of oxide dissolution becomes increasingly significant.

4. Discussion

4.1. Oxidation kinetics in different stages of the PEO process: classical approach

In the general case, the current density i passed through the oxide film during anodising can be represented as the sum

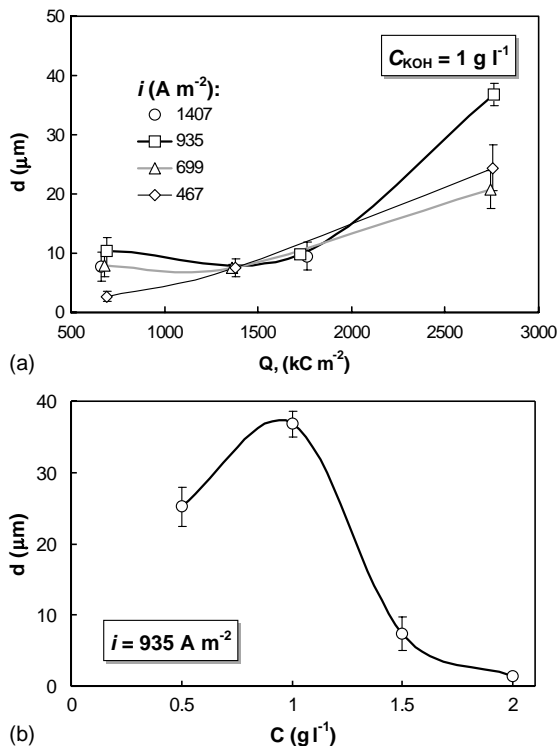


Fig. 7. Oxide layer thickness produced under different parameters of PEO, showing the effects of (a) charge density and (b) electrolyte concentration (time of electrolysis is 40 min).

of the partial processes of oxide film formation, dissolution and oxygen evolution at the anode surface:

$$i = i_i + i_e + i_d \quad (2)$$

where i_i is ionic current of the layer growth, i_e is the electron current caused particularly by the oxygen evolution and i_d is the anodic dissolution current. If the current yield of oxide formation is 100%, which is usually the case for conventional low-voltage anodising, then the total current is equal to the ionic one, i.e. $i = i_i$ and oxide film growth rate obeys the following equation [1]:

$$r_{\text{Al}_2\text{O}_3} = \frac{dU}{d\tau} = E \frac{M}{\rho n F} i = 5.68 \times 10^{-11} E i \quad (3)$$

Here M is alumina molar mass, $n = 6$, F , Faraday's constant and E , electric field intensity in the oxide film. Thus, when approximating galvanostatic (U) curves with linear dependencies, as shown in Fig. 2a, the oxide film growth rate can be evaluated in the framework of a conventional electrochemical approach. Values of $dU/d\tau$ for different stages of the PEO process are collated in Table 2 along with percentages of total charge density ($(Q_j/Q_\Sigma)100\%$) passed through the surface during each stages $j = \text{I–IV}$. As follows from Table 2, the major fraction of charge consumption in all experiments was during stage IV, where a plasma discharge is observed.

Data of field intensity E for each region of the galvanostatic curve calculated using data of Table 2 and Eq. (3)

Table 2
Characteristics of various stages of PEO process in 1 g l⁻¹ KOH solution

	Current density i (A m ⁻²)							
	467				700			
	Stage				Stage			
	I	II	III	IV	I	II	III	IV
$dU/d\tau$ (V s ⁻¹)	2.54	0.21	0.75	0.04	8.66	0.38	2.13	0.04
Q_j/Q_Σ (%)	1.1	13.3	17.2	68.4	0.7	4.7	5.9	88.6
	935				1407			
$dU/d\tau$ (V s ⁻¹)	14.4	0.4	2.01	0.04	16.7	1.67	4.41	0.06
Q_j/Q_Σ (%)	0.8	2.9	3.6	92.6	1.4	2.3	5.8	90.5

are presented in Table 3. For stage I, the value of $E_I = 4.04 \times 10^8$ V m⁻¹ is comparable with that given by Morlidge et al. [1] for 100% anodising efficiency (7.22×10^8 V m⁻¹). Assuming that in our case voltage gradient in region I corresponds to the oxide film growth with about 100% current yield, the process efficiency of anodic oxidation in other regions can be found from the following equation:

$$\eta_{\text{II,III,IV}}^{\text{an}} = \frac{(dU/d\tau)_{\text{II,III,IV}}}{(dU/d\tau)_I} = \frac{E_{\text{II,III,IV}}}{E_I} \quad (4)$$

Examples of calculations performed according to Eq. (4) are also given in Table 3, from which it follows that in regions II and III, both field intensity and oxide growth efficiency substantially decrease due to the collateral processes of metal dissolution and oxygen evolution. For the plasma discharge stage (region IV), this conventional approach ultimately leads to very low values of $\eta_{\text{IV}}^{\text{an}} = 0.15\%$, indicating that almost no anodic oxidation should take place on the electrode surface. This makes the net current efficiency of anodic oxidation in PEO also very low ($\eta^{\text{an}} = 2.2\text{--}7.2\%$), which is obviously underestimated, particularly taking into account data of Fig. 7.

4.2. Mechanisms underlying the oxidation kinetics during PEO

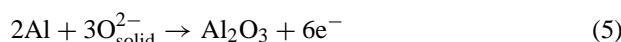
Dynamic equilibrium of partial processes of oxide formation, dissolution and oxygen evolution is quite common for aluminium anodising in alkaline solutions [13], where the following general reactions normally occur:

Table 3
Current efficiency of anodic oxidation process for various stages of PEO in 1 g l⁻¹ KOH solution

Part of galvanostatic curve	$dr_{\text{Al}_2\text{O}_3}/di$ ($\times 10^{-4}$, V m ² s ⁻¹ A ⁻¹)	E (V m ⁻¹)	η_j^{an} (%)
I	140	2.46×10^8	100
II	15	2.64×10^7	10.7
III	37	6.5×10^7	26.4
IV	0.2	3.5×10^5	0.15

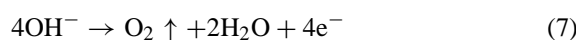
• Metal–oxide interface:

(i) anodic processes:

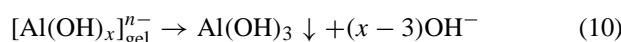
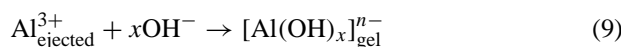
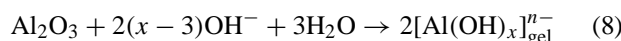


• Oxide–electrolyte interface

(i) anodic process:



(ii) alumina chemical dissolution and oxidation of ejected Al:



In non-agitated solutions the limiting stages are diffusion of OH⁻ anions to the electrode surface and chemical processes (8)–(10). When the solution is agitated (which is the case for the present study), the diffusion resistance can be disregarded and the process is (in the earlier stages) controlled, together with the chemical stages, by electrochemical ones, e.g. by reaction (5) at $C_{\text{KOH}} < 2$ g l⁻¹ or by (6) at $C_{\text{KOH}} \geq 2$ g l⁻¹ [15].

During the plasma stages of electrolysis (region VI), direct injection of Al into the electrolyte can occur through plasma discharge channels. The ejected Al is then immediately hydrolysed followed by hydroxide precipitation on the anode surface according to reactions (9) and (10). Acidification of the electrolyte solution discussed in Section 3.3. provides sufficient pH conditions in the vicinity of the anode for reaction (10) to occur. Subsequent plasma discharges dehydrate and re-crystallise the deposit, forming the oxide ceramic layer. The presence of such a plasma chemical route, involving reactions (9) and (10) in the net oxidation process, can thus provide an explanation of underestimated oxide growth efficiency, when the conventional electrochemical approach is applied alone.

Table 4
Kinetics of gas evolution during plasma electrolytic oxidation

PEO conditions	i (A m ⁻² at $C_{\text{KOH}} = 1 \text{ g l}^{-1}$)				C_{KOH} (g l ⁻¹ at $i = 935 \text{ A m}^{-2}$)			
	467	700	935	1407	0.5	1.0	1.5	2.0
r_{O_2} (ml s ⁻¹)	0.21	0.51	0.74	1.94	0.8	0.74	0.8	0.05 ^a

^a No plasma discharge observed.

4.3. Rate of gas evolution

Linear approximations of (V ; τ) dependencies shown in Fig. 3 allow estimation of the oxygen evolution rate r_{O_2} (ml s⁻¹) during PEO. Calculation results obtained using equation $r_{\text{O}_2} = dV/d\tau$, are shown in Table 4. Assuming also a linear dependence in (r_{O_2} ; i) coordinates, the following empirical equation for calculation of oxygen evolution rate has been obtained:

$$r_{\text{O}_2} (\text{ml s}^{-1}) = 1.8 \times 10^{-3} i (\text{A m}^{-2}) - 0.7702 \quad (11)$$

Both gas evolution observations and Table 4 data analyses have shown that the first gas bubbles begin to appear in stage II. The rate of gas evolution there is constant, corresponding approximately to 0.05 ml s⁻¹. This rate should be considered as the baseline rate of Faraday's oxidation process accompanied by partial dissolution, which occurs in 2 g l⁻¹ KOH solution without plasma discharge. In 0.5–1.5 g l⁻¹ KOH solutions, where plasma electrolytic stages are developed, the major gas volume evolves in stage IV. In this case, r_{O_2} is virtually independent of electrolyte concentration and can be adequately described by Eq. (11).

4.4. Current efficiency calculations for partial processes

Estimations of the process efficiency were carried out assuming that the partial processes of oxide film growth, dissolution and gas evolution on the surface are governed by the Faraday's law. Then, the balance equation for current yields of partial electrode processes on the anodic surface acquires the following form:

$$\eta_{\text{Al}_2\text{O}_3} + \eta_{\text{Al}_{\text{sol}}} + \eta_{\text{O}_2} = 100\% \quad (12)$$

where $\eta_{\text{Al}_2\text{O}_3}$, $\eta_{\text{Al}_{\text{sol}}}$, η_{O_2} represent current yields of alumina, dissolved metal and oxygen, correspondingly. Refer-

ence data used for the yield calculation of the electrolysis products are summarised by the set of Eqs. (13)–(15) presented in Table 5. Comparison of the calculation results with the experimental data of oxygen evolution rate (Fig. 3) shows that oxygen yield in the stages without plasma discharge corresponds to the rate of gas evolution according to reaction (15) but substantially exceeds this Faraday yield in the plasma stages of the process. For the latter stages, the amount of oxygen evolved by Faraday's law, was therefore, estimated as follows:

$$\eta_{\text{O}_2} = 100\% - (\eta_{\text{Al}_2\text{O}_3} + \eta_{\text{Al}_{\text{sol}}}) \quad (16)$$

Fig. 8 illustrates effects of current and charge densities on the PEO process efficiency in 1 g l⁻¹ KOH solution and the effect of electrolyte concentration can be traced in Table 6. It can be seen that the fraction of total current which is actually spent on the oxide film formation is always less than 1/3, indicating a range of PEO process efficiency at 10–30%. With increasing electrolyte concentration, alumina yield decreases and the proportion of dissolved metal increases, reaching eventually 1.1 and 30.9%, correspondingly, in 2 g l⁻¹ KOH solution. At this corner point of the experimental design, where plasma discharge stages cannot be achieved throughout the oxidation process, a material balance on the anodic surface corresponds approximately to 100% even with the value of η_{O_2} obtained using experimental data and equation (15). Thus the excess oxygen cannot be formed on the anode surface without a plasma discharge.

4.5. Formation of excess oxygen at the anode

The volume of excess oxygen $V_{\text{O}_2}^{\text{exc}}$ was found as the difference between total gas volume V_{O_2} (Fig. 3) and the calculated volume of oxygen produced via the Faraday reaction (15). In the studied range of current densities,

Table 5
Basic correlations used in current yield estimations for the main products of plasma electrolysis^a

Reaction	Electrochemical equivalent (q)	Current yield (η)	Equations
Anodic oxidation: $2\text{Al} + 3\text{O}_{\text{solid}}^{2-} \rightarrow \text{Al}_2\text{O}_3 + 6\text{e}^-$	$M/(6F) = 1.76 \times 10^{-4} (\text{g C}^{-1})$	$\delta S\rho/Qq_{\text{Al}_2\text{O}_3}$	(13)
Anodic dissolution: $\text{Al} \rightarrow \text{Al}_{\text{solid}}^{3+} + 3\text{e}^-$	$M_{\text{Al}}/(3F) = 9.32642 \times 10^{-5} (\text{g C}^{-1})$	$m_{\text{Al}}^{\text{sol}}/Qq_{\text{Al}}$	(14)
Oxygen evolution: $2\text{H}_2\text{O} - 4\text{e}^- \rightarrow \text{O}_2 + 4\text{H}^+$	$V_{\text{O}_2}^0/(4F) = 0.058 (\text{ml C}^{-1})$	$V_{\text{O}_2}/Qq_{\text{O}_2}$	(15)

^a Here M_{Al} is molar mass of aluminium; δ , oxide thickness; q_{Al} , $q_{\text{Al}_2\text{O}_3}$ and q_{O_2} , electrochemical equivalents of aluminium, alumina and oxygen, correspondingly; S , sample surface area and $V_{\text{O}_2}^0 = 22,400 \text{ ml}$, gas molar volume under normal conditions.

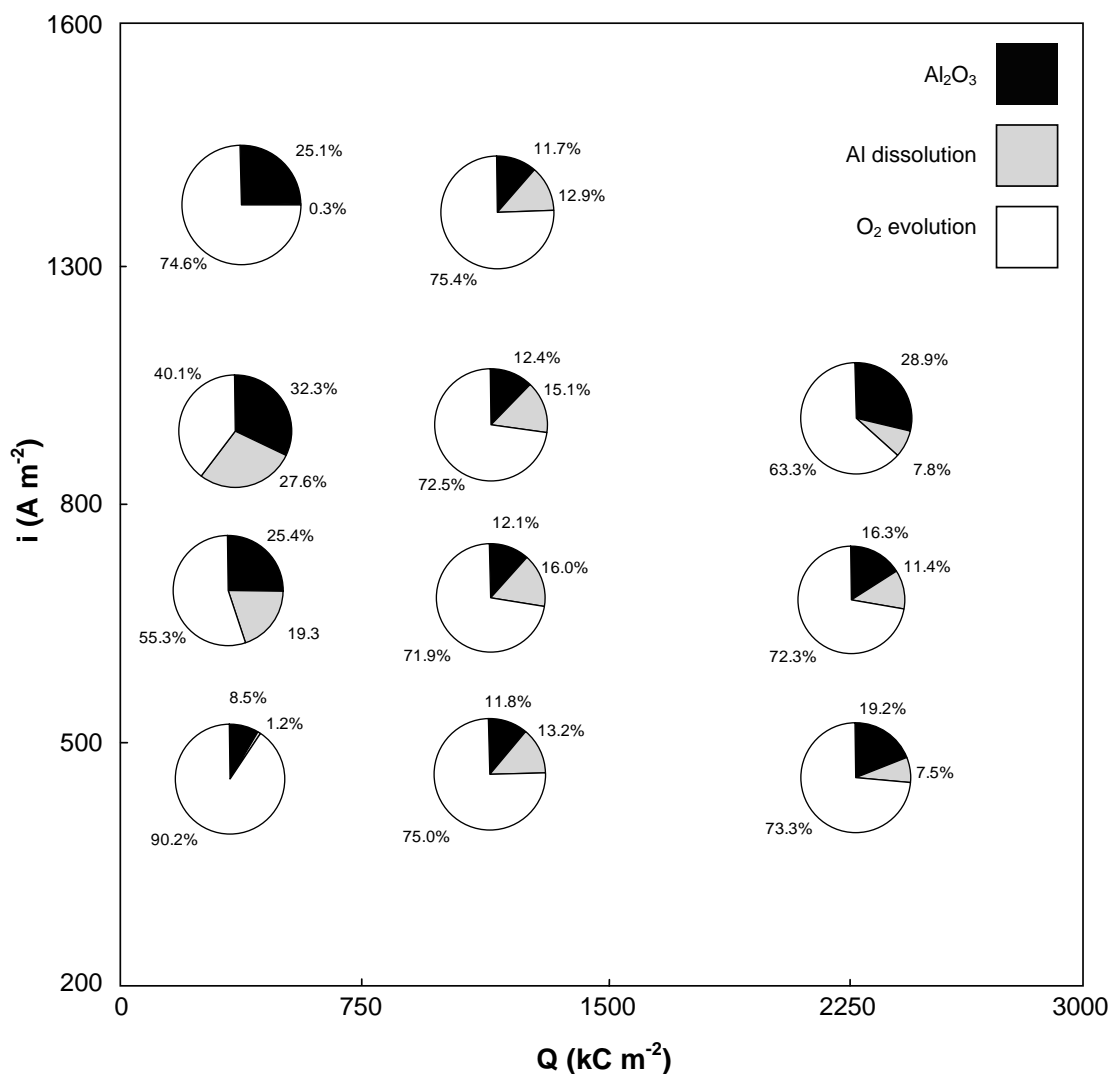


Fig. 8. Current efficiency diagram for partial anodic process in PEO of Al.

$V_{O_2}^{exc}$ is proportional to the charge passed through the cell (Fig. 9).

A substantial surplus of gas products over the expected Faraday yield has been reported in many other works dealing with plasma assisted electrolytic processes. A detailed overview of this issue has been presented by Bakovets et al. [9], from which it follows that the excessive gas liberation seems to be a generic feature of plasma electrolysis caused by fluxes of charged particles from the discharge

into the electrolyte. Gas formation is likely to occur in electrolyte areas adjacent to the discharge, particularly due to the reactions of H and O quadratic recombination. In alkaline solutions, this typically leads to linear

Table 6
Current yield of partial anodic products in plasma electrolytic oxidation

C_{KOH} (g l ⁻¹)	Oxidation $\eta_{Al_2O_3}$ (%)	Dissolution η_{Al} (%)	Gas liberation $\eta_{2,F}$ (%)
0.5	29.8	0.2	70.0
1	28.9	7.2	63.9
1.5	7.3	13.8	78.9
2	1.1	30.9	68.0 ^a

^a No plasma discharge observed.

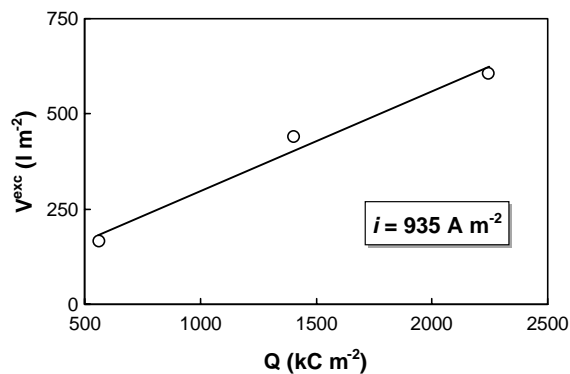


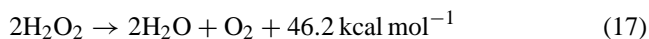
Fig. 9. Typical dependence of 'excessive' oxygen volume on charge density passed through the cell during PEO.

Table 7
Probable chemical reactions leading to occurrence of 'excessive' oxygen [20]

Reaction	Rate constant	
	($\text{l mol}^{-1} \text{s}^{-1}$)	(kJ mol^{-1})
$\text{H}_2\text{O}_2 + \text{e}_{\text{aq}}^- \rightarrow \text{OH}^- + \text{OH}$	1.2×10^{10}	15.1
$\text{O}_2 + \text{e}_{\text{aq}}^- \rightarrow \text{O}_2^-$	1.8×10^{10}	13.0
$\text{H}^+ + \text{e}_{\text{aq}}^- \rightarrow \text{H}$	2.3×10^{10}	12.2
$2\text{HO}_2 \rightarrow \text{H}_2\text{O}_2 + \text{O}_2$	8.3×10^5	24.7
$\text{O}_2^- + \text{HO}_2 \rightarrow \text{O}_2 + \text{HO}_2^-$	9.7×10^7	8.8
$\text{H}^+ + \text{OH}^- \rightarrow \text{H}_2\text{O}$	1.4×10^{11}	12.6
$\text{H}_2\text{O} \rightarrow \text{H}^+ + \text{OH}^-$	2.52×10^{-5}	45.4

dependencies of the gas evolution rate on total current density [9].

When assuming, following the work in ref. [9], that processes of electrolyte decomposition by plasma discharge in PEO are similar in nature to water radiolysis, a set of probable chemical reactions leading to the formation of excess oxygen can be suggested as shown in Table 7. As can be seen, one of the end products formed in the electrolyte under the discharge conditions is hydrogen peroxide, which has weakly acidic properties ($\text{pH} \approx 6$) and therefore, acidifies the electrolyte, as was observed in our experiments (Fig. 6). Direct determination of the peroxide in the electrolyte is impeded by its instability (and thus tendency to quickly dissociate into water and oxygen):



and, was therefore, not performed in this work. However, indirect evidence of H_2O_2 formation due to the plasma discharge is the fact that the solution pH decreased only if plasma stages of the process were achieved and remained otherwise unchanged (Fig. 6b).

Plasma discharges are well known to promote disintegration of molecular oxygen into atomic species; this also has been found during analysis of PEO gas products. However, the common by-product of the disintegration process, ozone could not be detected.

Another possible route for excess oxygen formation during PEO is thermal decomposition of water, which occurs via the following path:



However, due to the extremely strong bonds in the water molecule, its thermal dissociation proceeds very slowly, with 5.6 and 4.5% products formed at 2500 °C in the first and second steps, respectively. Dissociation of O_2 at this temperature is virtually insignificant but reaches 1.4 and 15% at 2700 and 3700 °C, respectively [21].

5. Conclusions

Investigations of the kinetics involved in the plasma electrolytic oxidation of Al in KOH solutions have revealed four stages of the process, characterised by different mechanisms of anodic reactions. Stage I corresponds to anodic oxidation of Al with approximately 100% current efficiency. In stages II and III, the oxide growth rate is substantially reduced due to the prevailing processes of anodic dissolution and phase recrystallisation of the oxide film. In stage IV, plasma chemical reactions at the anode–electrolyte interface govern the film growth.

Overall current efficiency of the oxide film growth lies within the 10–30% range and reduces significantly with increasing KOH concentration.

Oxygen evolution is the main electrochemical process at the potentials corresponding to plasma stages in the electrolysis. The total amount of oxygen liberated at the anode substantially exceeds the Faraday yield. This anomalous gas evolution is attributed to the radiolytic effect of plasma discharge events on the adjacent electrolyte volume.

Acknowledgements

Financial support of the work was provided by the UK Engineering and Physical Sciences Research Council (EPSRC) under project GR/R15696 and is acknowledged with thanks. The international collaboration became possible owing to support from the Royal Society. The authors are also grateful to Mr B. Knight for assistance with electrolyte analyses.

References

- [1] J.R. Morlidge, P. Skeldon, G.E. Thompson, H. Habazaki, K. Shimizu, G.C. Wood, *Electrochim. Acta* 44 (1999) 2423.
- [2] V.I. Chernenko, L.A. Snezhko, I.I. Papanova, *Coating by Anodic Spark Electrolysis*, Khimiya, Leningrad, 1991 (in Russian, ISBN 5-7245-0588-6).
- [3] P.S. Gordienko, S.V. Gnedenkov, *Microarc Oxidation of Titanium and its Alloys*, Dal'nauka, Vladivostok, 1997 (in Russian, ISBN 5-7442-0922-0).
- [4] V.I. Belevantsev, O.P. Terleeva, G.A. Markov, Y.K. Shulepko, A.I. Slonova, V.V. Utkin, *Z. Metall.* 34 (1998) 469 (in Russian, for English translation see *Protection of Metals*, ISSN 0033-1732).
- [5] A.L. Yerokhin, A.A. Voevodin, V.V. Lyubimov, J. Zabinski, M. Donley, *Surface Coat. Technol.* 110 (1998) 140.
- [6] I.V. Suminov, A.V. Apelfeld, A.M. Borisov, *Izvestiya RAS, Ser. Phys.* 64 (2000) 763 (in Russian).
- [7] J.-L. Delplancke, R. Winand, *Electrochim. Acta* 33 (1988) 1539.
- [8] J.-L. Delplancke, R. Winand, *Electrochim. Acta* 33 (1988) 1551.
- [9] V.V. Bakovets, O.V. Polyakov, I.P. Dolgovesova, *Plasma Electrolytic Anode Treatment of Metals*, Nauka, Novosibirsk, 1991 (in Russian, ISBN 5-02-029248-6).
- [10] A.V. Timoshenko, Y.V. Magurova, *Z. Metall.* 31 (5) (1995) 523 (in Russian, for English translation see *Protection of Metals*, ISSN 0033-1732).
- [11] V.N. Malyshev, A.G. Kolmakov, I.Z. Bunin, *Fizika i Khimiya Obrab. Mater.* 5 (1997) 77 (in Russian).

- [12] I.L. Rozenfeld, *Corrosion Inhibitors*, Khimiya, Moscow, 1977 (in Russian).
- [13] E.V. Koroleva, G.E. Thompson, G. Hollrigl, M. Bloeck, *Corrosion Sci.* 41 (1999) 1475.
- [14] S.-M. Moon, S.-I. Pyun, *Electrochim. Acta* 44 (1999) 2445.
- [15] B.N. Pautov, G.K. Lukonenko, L.A. Stenilovskaya, *Z. Metall.* 21 (1985) 475 (in Russian, for English translation see *Protection of Metals*, ISSN 0033-1732).
- [16] X. Zhou, G.E. Thompson, P. Skeldon, G.C. Wood, K. Shimizu, H. Habazaki, *Corrosion Sci.* 41 (1999) 1599.
- [17] Y. Lyu, P. Skeldon, G.E. Thompson, H. Habazaki, K. Shimizu, *Corrosion Sci.* 44 (2002) 1133.
- [18] J.S. Leach, C.N. Panagopoulos, *Electrochim. Acta* 32 (1987) 411.
- [19] M.M. Petrov, L.A. Mikheev, Y. Kukushkin, *Inorganic Chemistry*, Khimiya, Leningrad, 1981 (in Russian).
- [20] L.V. Bugaenko, V.M. Byakov, *High Energy Chem.* 32 (1998) 407 (in Russian).
- [21] *Chemistry Reference Book*, vol 1, B.P. Nikolskiy (Ed.), Khimiya, Leningrad, 1968 (in Russian).